The Astrophysical Journal, 653:725–732, 2006 December 10

HELIOSEISMICALLY DETERMINED NEAR-SURFACE FLOWS UNDERLYING A QUIESCENT FILAMENT

Bradley W. Hindman
JILA and Department of Astrophysical and Planetary Sciences, University of Colorado, Boulder, CO 80309-440; hindman@solarz.colorado.edu

Deborah A. Haber
JILA, University of Colorado, Boulder, CO 80309-440

and

Juri Toomre
JILA and Department of Astrophysical and Planetary Sciences, University of Colorado, Boulder, CO 80309-0440
Received 2006 May 2; accepted 2006 August 21

ABSTRACT

The extended filaments seen in Hα images of the solar disk, and the corresponding prominences when viewed at the solar limb, are one of the great hallmarks of solar magnetism. Such arches of magnetic field and the coronal plasma structures they support are both beautiful and enigmatic. Many models of filament formation and maintenance invoke the existence of surface plasma flows, which are used to drive the magnetic reconnection needed to form twisted loops of flux held down by a coronal arcade. These flows are typically composed of a converging flow, which brings flux elements of opposite polarity together, combined with a tangential shear that stresses the coronal arcade. In this paper we present helioseismic measurements of near-surface flows underlying a single quiescent filament lying within a decayed active region. Newly devised high-resolution ring analyses (HRRA) with both 2° and 4° spatial resolution were applied to Doppler imaging data provided by the Michelson Doppler Imager (MDI) instrument on the *SOHO* spacecraft. A long-lived filament appearing in 2002 May and April was studied. We find that the filament channel is a region of vigorous subphotospheric convection. The largest observed scales of such convection span the region of weak magnetic field separating the active region's two polarities. Thus, the magnetic neutral line that forms the spine of the filament channel tends to lie along the centers of large convection cells. In temporal and spatial averages of the flow field, we do not find a systematic converging flow. However, we do detect a significant shearing flow parallel to the neutral line. This shear takes the form of two oppositely directed jets, one to either side of the neutral line and within 20 Mm of the line. The jets produce a net shear in the flow speed of 30 m s^{-1} occurring over a distance of 20 Mm.

Subject headings: Sun: filaments — Sun: helioseismology

1. INTRODUCTION

The arching prominences that grace the limb have long been a source of scientific fascination, yet there persist fundamental questions about how these magnetic structures are formed and maintained (i.e., van Ballegooijen 2001). It is clear that prominences are ribbons of cool, dense plasma embedded in the hot, tenuous corona. Furthermore, they are located within a large, twisted magnetic structure that arches many tens of Mm above the surface (e.g., Martin 2001; Rust 2001). When observed on the solar disk in spectral lines such as Hα, the prominences appear as dark filaments overlying the chromosphere (Fig. 1*c*). The prominences and analogous narrow filaments are always located above the polarity inversion lines (neutral lines) separating regions with opposite magnetic polarity in the photosphere. They form in filament channels (Figs. 1*a* and 1*b*), which are regions where chromospheric fibrils are aligned parallel to the neutral line (e.g., Gaizauskas et al. 1997; Gaizauskas 1998, 2001; Martin 1998). Within the filament channel the magnetic field is mainly horizontal and directed along the neutral line. Quiescent prominences and filaments can persist for many days, but contain thread-like fine structure that often changes in a few minutes (Engvold 2001; Martin 2001; Lin et al. 2005).

The plasma in the prominence must be supported by magnetic fields with stable configurations that involve the bowed field lines first suggested by Kippenhahn & Schlüter (1957) and Kuperus & Raadu (1974). Recent prominence models that favor *flux ropes* involve an arched flux tube anchored in the photosphere at each end. The field lines in the corona make several revolutions about the axis to form a helix (e.g., Priest et al. 1989; van Ballegooijen & Martens 1989, 1990; Forbes 1990; Low 1993; Rust & Kumar 1994; Low & Hundhausen 1995; Kuijpers 1997; Chae et al. 2001; Gibson et al. 2004). The troughs in the field can support the cool prominence plasma, and the structure is stabilized by an overlying coronal arcade of field linking the two sides of the neutral line. The helical magnetic structure is created either by photospheric reconnection driven by footpoint motions that converge on the neutral line or by constructing the twisted flux rope in the convection zone and having it emerge as a fully formed entity. Modeling attention has also been devoted to explaining the observed preferred chirality (Martin et al.1994; Zirker 2001) of filament channels in the northern and southern hemispheres (e.g., Priest et al. 1996; van Ballegooijen et al. 1998, 2000; Martens & Zwaan 2001; MacKay & van Ballegooijen 2005).

An alternative scenario for prominences involves "sheared-arcade" models (e.g., Antiochos et al. 1994; DeVore & Antiochos 2000; Aulanier et al. 2002; Karpen et al. 2001, 2003) in which a narrow and strong magnetic shear straddles the neutral line, arising either from the action of photospheric flows parallel to that line, or from the emergence of preexisting sheared flux. The reconnection in this model occurs mainly in the corona. Much debate has occurred over which scenario for prominence formation

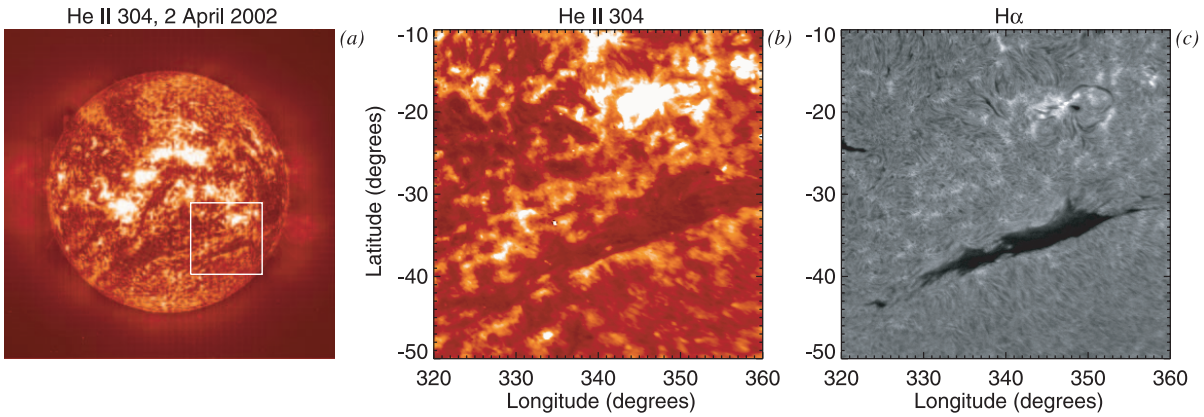

FIG. 1.—Magnetic structures in the solar corona. (*a*) Image of the solar disk in He II λ304 from the EIT instrument on *SOHO* taken on 2002 April 2. (*b*) Expanded view of the southwest corner (*lower right*) of (*a*), projected on a flat plane, showing a long filament channel that appears as a dark lane crossing from left to right. (*c*) Hα image taken on the same day by BBSO. The long black filament is part of the larger filament channel that appears in the EIT images.

should be preferred, as the different magnetic structures that result have implications for theories of coronal mass ejections (CMEs) and eruptive flares (e.g., Forbes 2000; Klimchuk 2001; Low 2001; Moore 2001).

The high electrical conductivity of the solar plasma, whether in the atmosphere or in the interior, implies close coupling between flows and magnetism. Deep within the solar interior, gas pressure dominates the magnetic pressure, and the magnetic field is readily advected by the flow. Within the corona the situation reverses and the fluid is strongly constrained to slide along the field lines. The photosphere and near-surface regions are zones of transition for such behavior, having notable forces exerted by flows on magnetic fields and vice versa. Thus, we expect interactions between flows within the near-surface shear layer and the magnetic field within the photosphere and corona. Helioseismic observation of such flows has already revealed an intimate connection between subsurface flows and the presence of magnetic active regions and sunspots (e.g., Gizon et al. 2000, 2001; Haber et al. 2000, 2002; Zhao et al. 2001).

In this paper we present the first evidence that such subsurface flow fields are correlated with the existence of coronal filaments. In § 2 we discuss the helioseismic technique used to analyze the subsurface flow field. The flows underlying a particular filament observed over four days in the year 2002 are presented in § 3 and a discussion of our findings appears in § 4.

2. HIGH-RESOLUTION RING ANALYSES (HRRA)

Helioseismic ring analysis assesses the speed and direction of horizontal flows below the solar surface by measuring the Doppler shift of ambient waves that are advected by the flow field. For this study we have employed surface gravity waves (*f* modes). Waves traveling in opposite directions have their frequencies split by the Doppler effect when a flow is present, providing a direct measure of the flow velocity in those layers where the *f* mode has a significant amplitude. The frequency perturbation introduced by the flow is $\Delta\omega = \boldsymbol{k} \cdot \boldsymbol{U}$, where $\boldsymbol{k}$ is the horizontal wavenumber and $\boldsymbol{U}$ is the integral over depth of the horizontal flow velocity weighted by a kernel that is approximately the kinetic energy density of the surface gravity wave.

The frequency splittings produced by flows are measured in the Fourier domain. For a single analysis, a power spectrum is obtained of the wave field in a localized region on the solar surface by Fourier transforms (two in space, one in time) of a sequence of tracked, remapped, and apodized Dopplergrams (Bogart et al. 1995; Haber et al. 1998). The mode power in the spectrum is distributed along curved surfaces, which when cut at a constant frequency appears as a set of concentric rings, each ring corresponding to a mode of different radial order. These rings are nearly circular in shape and possess centers that are displaced slightly from the origin due to the splitting of the mode frequencies. Figures 2*a* and 2*b* show how the rings appear for two different frequencies using a small 2° region. The outermost ring corresponds to the *f* mode and the inner rings correspond to the acoustic *p* modes, p_1, p_2, and so forth. Figure 2*c* shows a profile of the power spectrum as a function of frequency at a particular value of the wavenumber vector. Notice that the *f* mode and p_1 ridge are clearly visible, as is the p_2 mode. For this study, we carefully fit the *f* modes in such power spectra with Lorentzian profiles to obtain

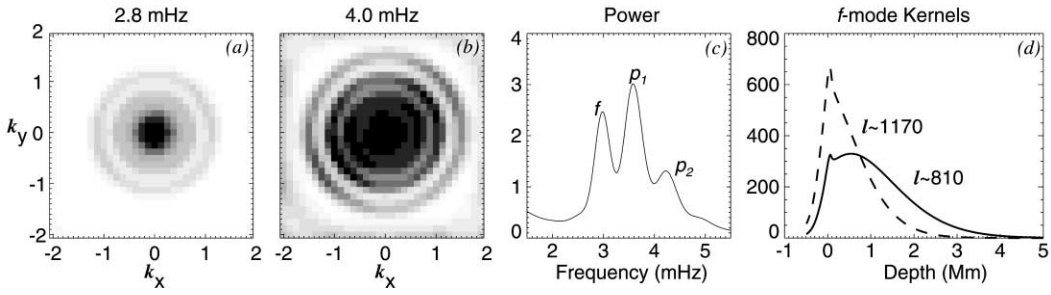

FIG. 2.—Sample power spectra for 2° tiles observed for 27.7 hr and averaged over many different tiles. (*a*)–(*b*) Two sections through the 3D power spectra at constant temporal frequency. The outermost ring corresponds to the *f* mode and the inner rings to the acoustic *p* modes, p_1, p_2, and p_3. (*c*) Profile of the spectra as a function of temporal frequency for a constant value of the horizontal wavenumber vector. (*d*) The sensitivity kernels for two *f* modes with harmonic degrees $\ell = 810$ and 1170, plotted as a function of depth below the photosphere. Each kernel is approximately equal to the mode's energy density and each samples the upper 2 Mm of the convection zone.

the frequency splittings as a function of horizontal wavenumber (e.g., Haber et al. 2000, 2002).

A single ring analysis is performed within a small region, or tile, on the solar surface. The resulting flow is an average measure of the flow within that tile. We map the flow field over the entire visible disk by performing many ring analyses at different locations over the same period of time. The flow field can then be studied as a function of time by repeating the analysis over the entire mosaic of tiles for later dates.

For this study, we have used Dynamics Program data from MDI (Scherrer et al. 1995) on the *SOHO* spacecraft. We have adapted the analysis scheme described by Haber et al. (2002) to measure small-scale flows and call the new procedure high-resolution ring analysis (HRRA). Previous ring analyses have tracked a mosaic of 189 separate regions across the solar surface. Each region is square, 16° on a side, and is tracked for 27.7 hr at the local rate of rotation for the surface (Snodgrass 1984). The tile centers are separated by 7.°5 in latitude and longitude. The mosaic of tiles fills the solar disk out to roughly 60° from disk center. For the present study we use this same tracking and tiling scheme for efficiency. However, instead of performing the ring analyses on each tracked tile, and achieving the standard measurement resolution of 16°, each of the large tracked regions is dissected into a multitude of smaller tiles. We measure flows on two different submosaics: one is composed of square tiles that are 4° in heliographic angle on a side, while the other has tiles that are 2° on a side. In the remapped images, these two scales correspond to subimages that are 32×32 pixels and 16×16 pixels, respectively. After extraction from the larger tracked region, each of the subtiles is apodized to a circular disk.

The small tiles are packed within the tracked regions such that the tiles overlap. For the 4° tiles, the tile centers are separated by 1.°875 in latitude and longitude, whereas the centers for the 2° tiles are separated by 0.°9375. From a single 16° tracked region, we extract either 225 tiles of 2° or 49 tiles of 4°. Since the large tracked regions are 16° on a side and are separated from each other by only 7.°5, the tracked tiles also overlap. When extracting small tiles, the same site of the solar surface typically appears within four different tracked regions. We extract all four regions and process each separately. This provides four realizations of the flow field at that location, which we subsequently average together. The variance in all velocities measured at the same location on the Sun, but extracted from different tracked regions, is comparable to the uncertainty due to random errors.

The spatial resolution achieved by this technique is largely determined by the size of the tile and the shape of the apodization function. In the limit of large wave damping, when waves do not travel across the analysis tile before dissipating, the measured flow is approximately an average of the local flow field weighted by the square of the apodization function (Hindman et al. 2005; Birch et al. 2006). In these analyses we have used a circular apodization that is flat within a specified radius and possesses a rather sharp, beveled edge. Therefore, the flow is essentially an average over a disk with a relatively even weighting within that disk. By design the tiles have been apodized to disks with radii similar to the tile spacing: 1.°875 for the 4° tiles and 0.°8750 for the 2° tiles.

Vertically, the spatial resolution is controlled by the eigenfunction of the measured *f* mode. Since the *f* modes are surface gravity waves, they are confined to a narrow layer just below the solar surface. Depending on the mode's horizontal wavenumber, the peak of the energy density varies from being directly at the surface to 1 Mm below. The eigenfunction spans only the first 2 Mm below the surface. Figure 2*d* presents two *f*-mode eigenfunctions for the extremes of the range of fitted wavenumbers (roughly 800–1200 in harmonic degrees).

The exact depth to which the eigenfunction extends is proportional to the horizontal wavelength. However, the small tiles used in this study only allow a small range of wavelengths to be measured. Thus, the vertical eigenfunctions of all the measured *f* modes are rather similar. This property allows us to improve our signal-to-noise ratio by averaging the frequency splittings measured for *f* modes of different wavelengths. Typically, 10 different wavelengths can be fit for spectra obtained from the 4° tiles whereas only three or four can be gleaned from spectra of 2° tiles.

The averaging over wavenumbers and over realizations (obtained from different tracked regions) is important because it reduces the measurement errors substantially. Simultaneously during the fitting, an estimate of the uncertainty in each frequency splitting is obtained from the broadness of the minima in χ^2, the goodness of fit. Assuming that the errors are uncorrelated, after averaging the velocities, a typical fractional uncertainty is 20% for the 2° tiles and 0.5% for the 4° tiles. The small uncertainty for the 4° tiles is an outcome of the large number of *f* modes with different wavenumbers that can be fit and the inherently smaller random errors achieved for larger tiles.

3. FLOWS UNDERLYING A FILAMENT

Flow maps are generated by repeating the helioseismic analysis on many different small regions distributed across the solar disk and by repeating the entire mosaic of analyses once each day. Figure 3*a* shows the results of such a mapping procedure applied to 27.7 hr of MDI data starting on 2002 March 29. The tiles used in this analysis are 4° in diameter. The map reveals a systematic convective pattern of outflow sites in the quiet Sun with the magnetic field concentrated in the lanes between convection cells. While resembling supergranulation, the convective cells seen in Figure 3 are about fourfold larger than the typical supergranule. This predominant scale is preferentially selected by the ring analyses because the size of the analysis tiles (4° or 45 Mm on a side) averages over all smaller scales. (See § 4.1 for a deeper discusion of this issue.) Figure 3*b* shows a colocal Hα image taken during the period of the helioseismic observations. The slender filament appearing in the southern hemisphere near 340° in longitude is the same filament illustrated in Figure 1*c*, just imaged a few days earlier.

The structure of the flow field near the filament is complicated and evolving. Therefore, in Figures 4 and 5 we present magnified views of the region outlined in Figure 3 with a dashed white box. Both Figures 4 and 5 present the flows over four consecutive days in 2002 using, in turn, 4° and 2° tile resolutions. The further-reduced field of view in Figure 5 is indicated by the dashed white box in Figure 4.

Unlike the simple prediction posited by several models of filament formation, a simple inflow along the magnetic neutral line is not seen. Instead, the flow field is rather complex and has several long-lived convection cells spanning the filament channel. The locations of the central upwelling and outflows associated with these cells are indicated by the numerals I–IV. Although only the four cells that are cospatial with the filament channel are marked, clearly others also exist. Over the 4 day interval, the flow field evolves—convergence lanes and cell boundaries form, disappear, and migrate. This temporal evolution is more evident in Figure 5 with its finer horizontal resolution. However, even for the flows obtained with 2°-diameter tiles, the four outflow sites more or less persist throughout the 4 days (as do many other sites unrelated to the filament). These cells are not canonical supergranules, which are typically 20 Mm in diameter (or 1.°6 in heliographic

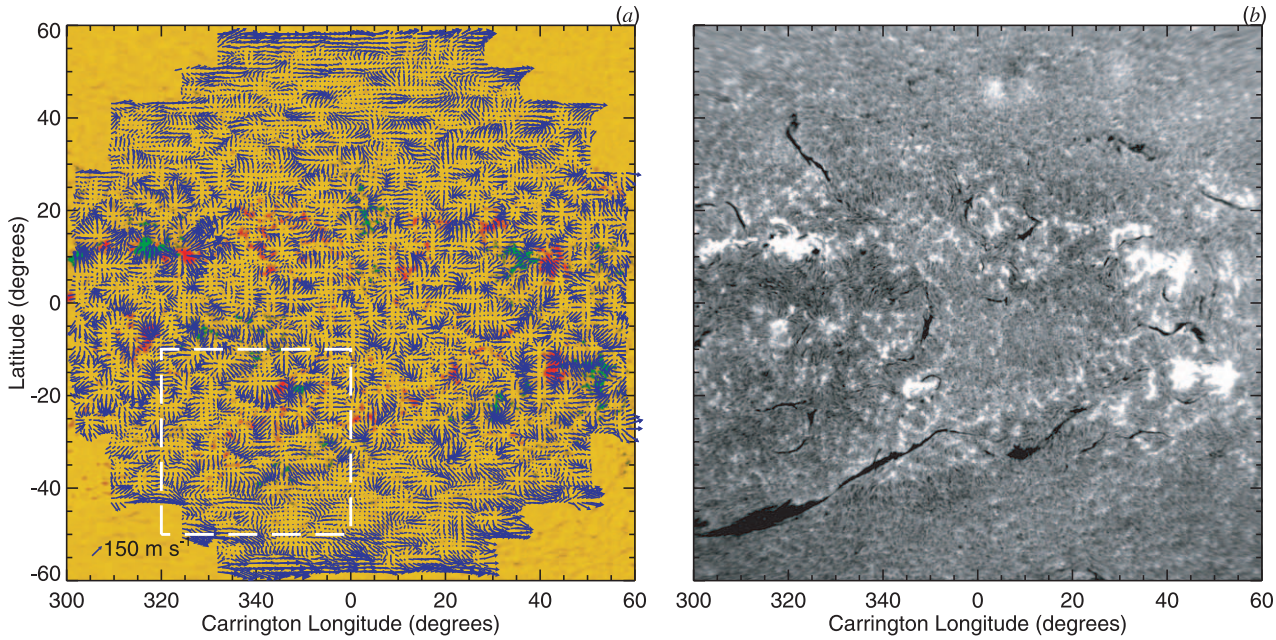

FIG. 3.—Flows deduced using HRRA for a single day of MDI data (2002 March 29). (*a*) Map of flows measured using only *f* modes. Each of the individual analysis domains are 45 Mm on a side or roughly 4° in heliographic angle. Flow velocity errors are on the order of 15 m s^{-1}. The red and green tones indicate magnetic fields of opposite polarity. The flows form a distinct cellular structure with cell boundaries strongly correlated with the regions of intense magnetic field. (*b*) Hα image taken at BBSO during the same day. The long filament appearing in the lower left corner is studied in more detail in Figs. 4–6.

angle). The size of the analysis tiles (4° and 2° in diameter) averages over this spatial scale. Hence the observed cells, which are roughly 6° (≈80 Mm) in diameter, are considerably larger than most supergranules. Their size may be controlled by the separation of the regions of opposite polarity plage, which is a vestigial remnant of the decayed active region in which the filament channel is embedded.

Careful averaging of these flows does reveal the presence of large-scale flows associated with the magnetic neutral line. However, as one might expect from the existence of convection cells that are predominantly outflows, these large-scale flows are not converging on the neutral line. Careful arrangement and alignment of the outflow cells and their boundaries would be required to form a zone of convergence at the neutral line. By averaging the flows over four days and in one spatial dimension (along the neutral line), we obtain an average flow field as a function of distance from the neutral line. Figure 6*a* shows a magnetogram of the region with the projection of the filament on the solar disk indicated by a solid blue curve (as seen in Big Bear Solar Observatory [BBSO] Hα images). The thin black curve marks the location of the neutral line, and the dashed black line is a straight-line fit to the neutral line within the region indicated by the white box. The flow field is averaged along the dashed black curve and over the four days 2002 March 30–April 2. We then decomposed this average flow into a component parallel to the neutral line (or its straight-line approximation) and a component that is perpendicular to the line. The parallel component is shown in Figure 6*b* as a function of distance from the neutral line (in degrees) and the perpendicular component appears in Figure 6*c*. For each measured speed, the small black error bars denote the formal measurement uncertainties of the average (derived from the formal mode fitting errors). The larger red bars simply indicate the day-to-day variance of the flows. That variance is the result of the evolution of the fast convective flows, which have been largely (although not completely) removed by the averaging procedure.

For this filament, the average flows do not evince an obvious convergence or divergence of the perpendicular flow component. However, there is clear evidence for a shear across the neutral line in the parallel component. To either side of the neutral line (within 2° or roughly 20 Mm) there appears a jet, with speeds of 10 and 20 m s^{-1}. The two jets are directed in opposite directions, thereby generating a shearing flow with a magnitude of 30 m s^{-1} over a distance of 20 Mm.

4. DISCUSSION

We must keep in mind that the present study has only examined the flows in the vicinity of a single filament. Furthermore, the flows are only representative of a single stage in this particular filament's lifetime. The filament first appeared already formed on 2002 January 27 as the Sun's rotation carried it over the eastern limb. Born in NOAA Active Region 9802, the filament persisted for five complete rotations, suffering several large eruptions during that time. Of particular interest is that two CMEs associated with the filament under study occurred on each of the dates 2002 April 1 and April 4. The first date lies in the middle of our period of observation and the later date several days afterward.

4.1. *Convection within the Filament Channel*

The flows within the filament channel do not consist of the simple, slowly varying flows often posited by models of filament formation. Instead the flows are highly dynamic, changing from day to day and with high spatial variability. The dominant flow structures observed within the filament channel itself are large-scale convection cells. The spatial resolution of helioseismic measurements precludes measuring flows smaller than roughly 20 Mm in scale; therefore, cells the size of a typical supergranule are not visible, although such flows are surely present. Instead the dominant cell size is roughly 80 Mm. This distance is similar to the separation between regions of significant photospheric magnetic flux to either side of the filament channel.

Recent 3D simulations of turbulent solar convection in full, spherical shells (Brun et al. 2004) are revealing convection with

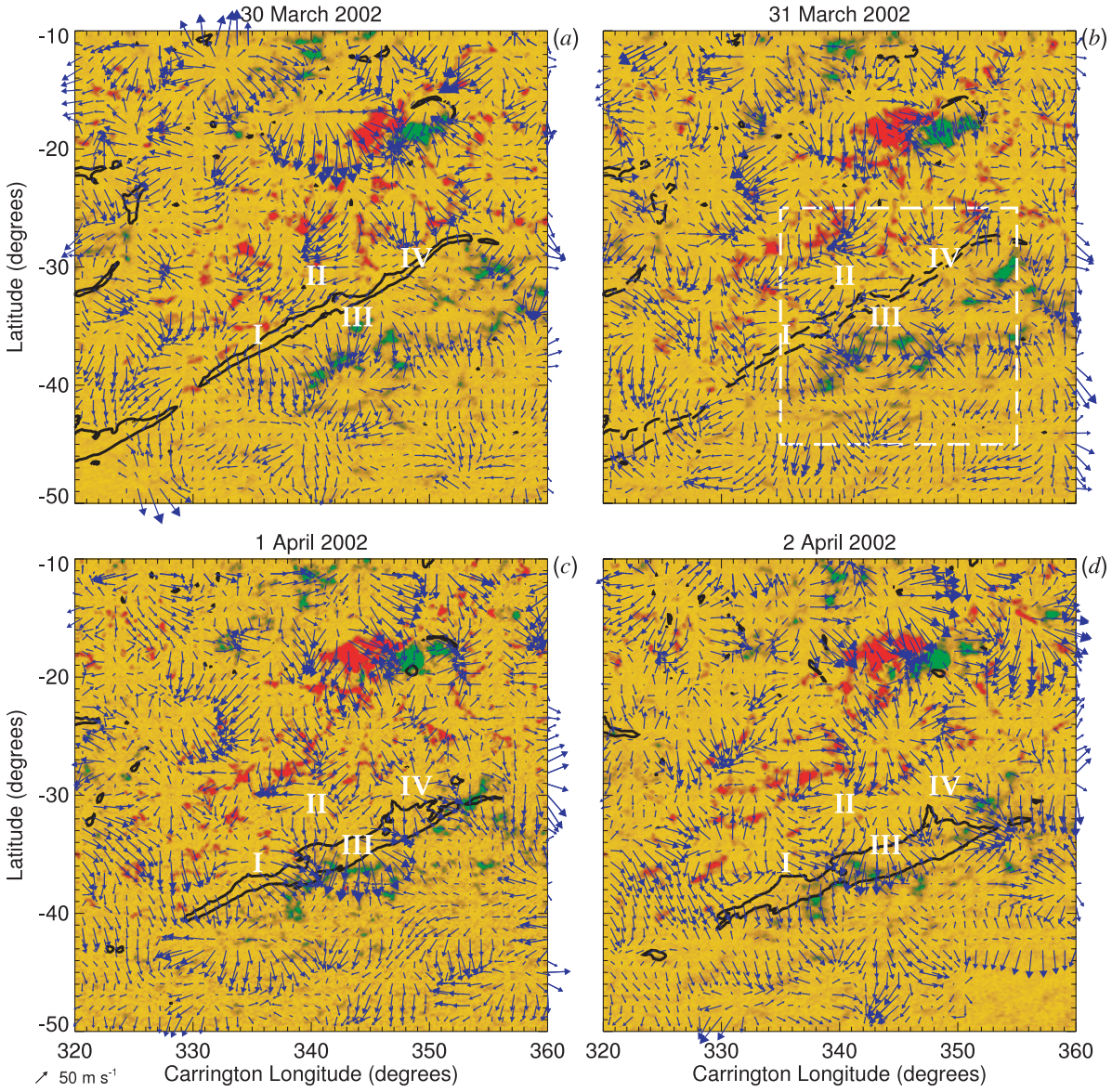

FIG. 4.—Daily high-resolution flow maps obtained using 4°-diameter tiles. The maps span four consecutive days: (*a*) 2002 March 30, (*b*) 2002 March 31, (*c*) 2002 April 1, and (*d*) 2002 April 2. Regions of opposite magnetic polarity, as determined from MDI magnetograms, are indicated in green and red. The dark contour line shows the position of a filament as observed in BBSO Hα images. On March 31when BBSO images were unavailable, the contour from the previous day is indicated with a dashed line. Four long-lived convection cells span the location of the filament and are marked with numerals I–IV (in white). The filament runs through the center of these cells and the apparent flow along the neutral line is complicated. The widening of the filament over the span of the four days is probably due to projection of the filament against the solar disk as the region rotates across the Sun's visible surface.

a wide range of scales, including the ones seen in this study. Furthermore, we know from direct Doppler observations of solar convection (Hathaway et al. 2000) that the Sun evinces a wide range of convective motions, with supergranulation and granulation both being broad peaks in the spectrum of such flows. For flows with a spatial scale larger than the canonical scale of supergranulation ($\ell = 120$) the convective spectrum is a rapidly decreasing function of size. Therefore, any procedure which acts as a low-pass filter (which any helioseismic technique does) will be primarily sensitive to the smallest scale motions that it can resolve. Hence, with our HRRA technique within the quiet Sun we typically see convection cells that are roughly twice the size of the tiles used. Smaller scale flows are simply filtered out revealing the larger scales of solar convection that are otherwise masked because of their slow speeds.

It has long been known from correlation tracking and direct Doppler velocity observations that magnetic field concentrates at the boundaries of supergranulation cells. More recently, helioseismic studies have revealed that the surface magnetic field and large-scale subsurface flows are highly correlated (Gizon et al. 2001; Haber et al. 2001, 2002). Therefore, it is not surprising that the large convection cells observed within the filament channel are correlated with the surrounding magnetic field. It is interesting, however, that the preferred cells are those that completely span the weak-field region near the magnetic inversion line. In the case of supergranulation in the quiet Sun, it is clear that the magnetic field gathers at the boundaries between convective cells. The convection appears to sweep out the cell interiors, advecting the field to the boundaries where it accumulates in the downflow sheets and interstices. For larger scale convection, which has

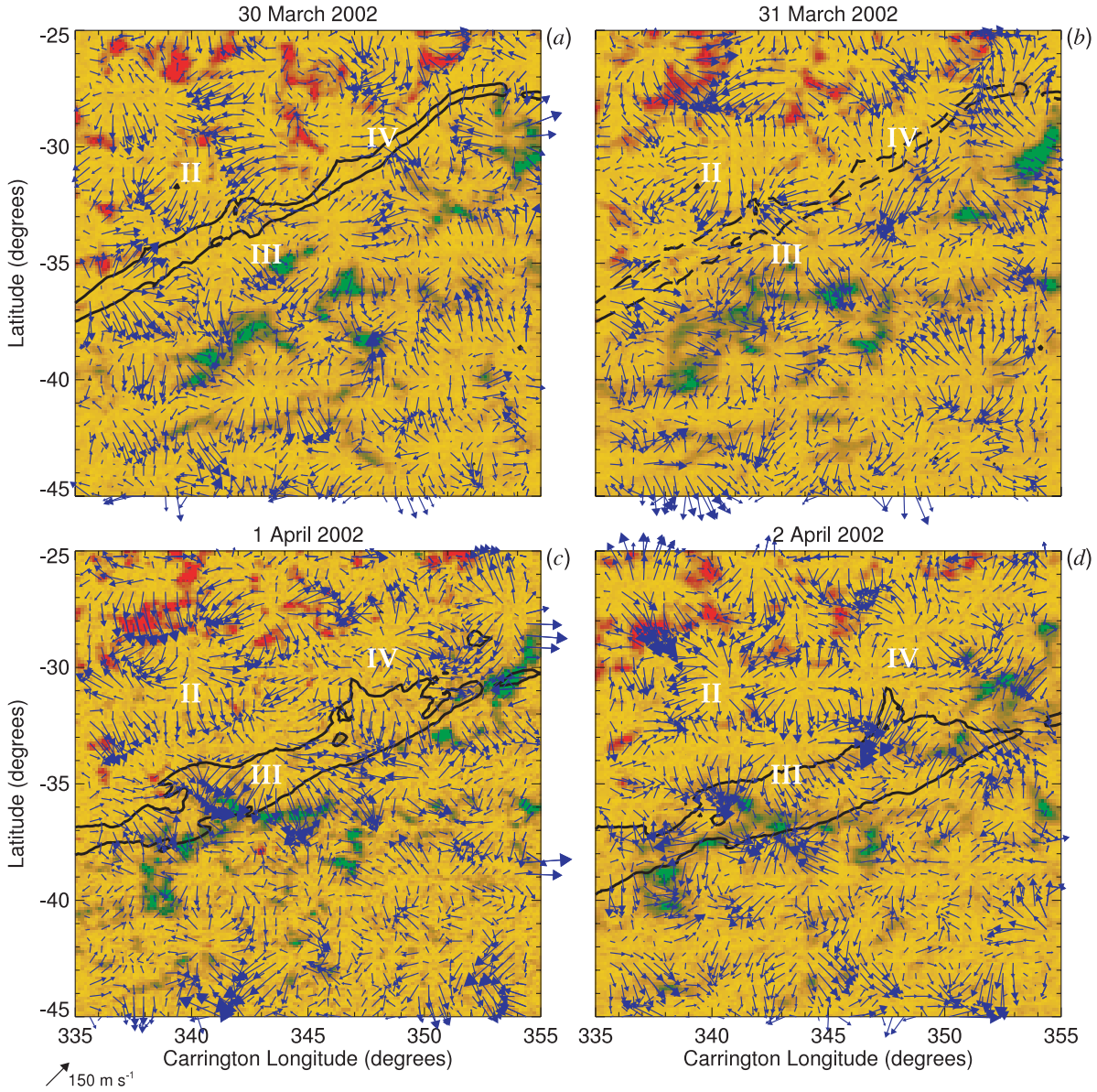

FIG. 5.—Daily high-resolution flow maps obtained using 2°-diameter tiles, zoomed in to cover the region outlined with the white dashed box in Fig. 4*b*. The maps span the same four days displayed in Fig. 4: (*a*) 2002 March 30, (*b*) 2002 March 31, (*c*) 2002 April 1, and (*d*) 2002 April 2. The finer resolution available in these maps indicate that there is a complex interaction between the flow cells and photospheric magnetism.

longer lifetimes and slower flow speeds, it is not clear whether the same process is at work. It could very well be that the size and shape of the convection itself is partly regulated by magnetic stresses.

The observed cells persist for all of the 4 days of helioseismic observation, although significant changes in their shape and intensity occur over that period. It is also evident from the flows obtained with 2° tiles that several of the cells fractured and new cells appeared. The observed lifetime of these cells is consistent with previous measurement of supergranules (DeRosa & Toomre 2004). Whereas the typical supergranule lives for about a day, larger supergranules may last for 3 or 4 days.

Many models of filament formation and evolution invoke the existence of flows that converge on the magnetic neutral line. Such flows are desirable, such that magnetic flux elements of opposite sign are brought together in order to reconnect and thereby restructure the magnetic field in the corona. For the filament we have examined here, such a converging flow is not evident. In fact, there is weak evidence for a diverging flow on the average (see Fig. 6). While a large-scale converging flow is one of the simplest mechanisms for bringing magnetic elements of opposite alignment together, other possibilities exist. The convection that we observe within the filament channel may also be a viable mechanism (Amari et al. 2003). Turbulent diffusion caused by supergranulation and other scales of convection could transport flux from where the field is strong to where it is weak. Of course, this is just the direction that is required to mix together flux elements from outside the filament channel. The stronger magnetic flux outside the channel will tend to diffuse into the weak-field region of the filament channel, where it can reconnect with oppositely aligned flux brought in by diffusion from the other side of the channel. Typical estimates and measurements of diffusion arising from turbulent convection in the photosphere give rise to long-term diffusion coefficients D, ranging from 250 $\mathrm{km^2\ s^{-1}}$ (Hagenaar et al. 1999) to 600 $\mathrm{km^2\ s^{-1}}$ (Schrijver et al. 1996). A rough estimate of the transport of magnetic flux by such diffusion

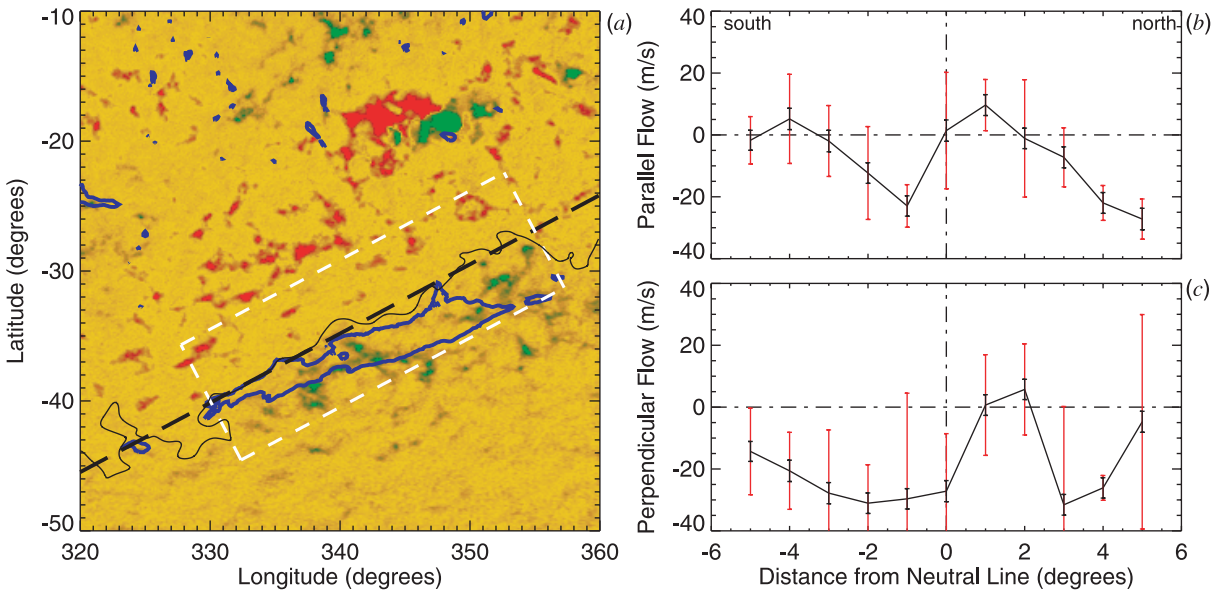

FIG. 6.—Large-scale flows associated with the filament, achieved through spatial and temporal averaging. (*a*) Magnetogram from 2002 April 2 obtained with MDI, with a contour of the magnetic neutral line (*thin black curve*) and a contour of a cospatial BBSO Hα image showing the location of the filament (solid blue curve). The black dashed line indicates a straight-line fit to the neutral line within the region enclosed by the white dashed box. The flows depicted in Fig. 5 were averaged along the filament within the white box and averaged over the four days 2002 March 30– April 2. The flows within 5° of the axis have been decomposed into (*b*) a component parallel to the axis and (*c*) a component perpendicular to the axis and then averaged along the axis. A positive velocity corresponds to roughly prograde flow in the parallel component and nearly northerly flow in the perpendicular component. The black error bars indicate the formal error estimates, while the red bars show the day-to-day variance in the flows.

across a filament channel with a width L, equal to 20 Mm, indicates that an inflow of 25 to 60 m s^{-1}, respectively, would be required to cause a comparable convergence of magnetic flux ($v_{\rm in} = D/L$). Although the averaged flows observed in this study do not display a systematic convergence or divergence on the neutral line, the magnitude of the mean flows is quite comparable to the diffusive speed estimated here. Therefore, if further studies find filaments that do possess an observed inflow, both advection and diffusion of magnetic flux are likely to play a major role in feeding the neutral line with elements of opposing magnetic flux.

4.2. *Nature of the Observed Shear*

The temporal and spatial averages of the flows displayed in Figure 6 show no indication of a flow that converges on the magnetic inversion line. However, Figure 6*b* does exhibit an average shear in the parallel component. To either side of the neutral line there exists a jet, and taken together the jets have an anticyclonic sense. The jet north of the neutral line is directed westward (prograde) with a speed of roughly 20 m s^{-1}, while the southern jet is directed eastward (retrograde) with a weaker speed of 10 m s^{-1}. The structure of both jets is underresolved, but they each have a width no greater than 2° in heliographic angle or 20 Mm. The net shear across the neutral line, from the peak of one jet to the other, is roughly 30 m s^{-1} occurring over a distance of only 2° or 20 Mm.

If a coronal arcade had footpoints to either side of the neutral line, separated by 20 Mm, and the magnetic field joining those points was initially perpendicular to the neutral line, such a shear, through differential advection of the footpoints, would stretch and twist the field lines. The angle between the neutral line and the arcade field would initially grow by about 7° per day. The stress placed on the coronal arcade by such a shear flow is not insignificant. Over several days, if left unimpeded, the shear flow can sufficiently stress the overlying magnetic arcade to destabilize the filament's magnetic structure.

4.3. *Reflections*

Enabled by our new HRRA procedures, the present study has revealed two properties of the subsurface flows in the vicinity of a solar filament and its underlying filament channel: (1) there is vigorous and fairly persistent convection evident in the region surrounding the magnetic neutral line, and (2) long-term averages reveal a prominent shearing flow aligned with the neutral line. These aspects provide support for models requiring shear in order to form and maintain filaments. Furthermore, the presence of complex cellular flows crossing the neutral line implies magnetic field entanglements that are not an element in most simplified models.

Since we have only examined a single filament over a 4 day interval, we cannot yet say whether these findings will be ubiquitous for all filaments. Nor can we say whether the observed flows are typical for filaments only in one particular stage in their lifetime. We are planning new studies in which the flows will be measured for a large number of filaments, and in which the structure and nature of the flow field will be characterized as a function of the filaments' level of activity and stage of life. However, such an effort is a major undertaking. To produce a flow map for a single day (such as appears in Fig. 3), over 4000 separate Dopplergram power spectra must be computed, fitted, and averaged. With the advent of data from the Helioseismic and Magnetic Imager (HMI), which will be aboard the *Solar Dynamics Observatory* (*SDO*), the computational load will only increase. HMI will boast a threefold-finer spatial resolution than the present MDI instrument. We fully expect that such an increase in resolution will permit direct sampling of flows with a spatial scale comparable to supergranulation. More importantly, we should be able to resolve the region lying directly underneath the filament channel.

We thank Sarah Gibson, Giuliani de Toma, Marc DeRosa, and Patrick McIntosh for useful advice and discussions. We

thank Richard Bogart for his substantial efforts in tracking and remapping the MDI data for use in ring analyses. We thank Ben Brown and Gwen Dickinson for their help in preparing this manuscript. This work was supported in part by NASA through grants NAG5-11920, NAG5-12491, NAG5-13520, NNG05G124G and NNG05GM83G, and by the NSF through grant ATM-0219581.

REFERENCES

Amari, T., Luciani, J. F., Aly, J. J., Mikic, Z., & Linker, J. 2003, ApJ, 595, 1231
Antiochos, S. K., Dahlburg, R. B., & Klimchuk, J. A. 1994, ApJ, 420, L41
Aulanier, G., DeVore, C. R., & Antiochos, S. K. 2002, ApJ, 567, L97
Birch, A. C., Gizon, L., Hindman, B. W., & Haber, D. 2006, ApJ, in press
Bogart, R. S., Sá, L. A. D., Duvall, T. L., Jr., Haber, D. A., Toomre, J., & Hill, F. 1995, in Proc. 4th *SOHO* Workshop, Helioseismology, ed. J. T. Hoeksema et al. (ESA SP-376; Noordwijk: ESA), 147
Brun, A. S., Miesch, M. S., & Toomre, J. 2004, ApJ, 614, 1073
Chae, J., Wang, H., Qiu, J., Goode, P. R., Strous, L., & Yun, H. S. 2001, ApJ, 560, 476
DeRosa, M. L., & Toomre, J. 2004, ApJ, 616, 1242
DeVore, C. R., & Antiochos, S. K. 2000, ApJ, 539, 954
Engvold, O. 2000, Encyclopedia of Astronomy and Astrophysics, ed. P. Murdin (Bristol: IOP)
Forbes, T. G. 1990, J. Geophys. Res., 95, 11919
———. 2000, J. Geophys. Res., 105, 23153
Gaizauskas, V. 1998, in IAU Colloq. 167, New Perspectives on Solar Prominences, ed. D. Webb, B. Schmieder, & D. Rust (ASP Conf. Ser. 150; San Francisco: ASP), 257
———. 2000, Encyclopedia of Astronomy and Astrophysics, ed. P. Murdin (Bristol: IOP)
Gaizauskas, V., Zirker, J. B., Sweetland, C., & Kovacs, A. 1997, ApJ, 479, 448
Gibson, S. E., Fan, Y., Mandrini, C., Fisher, G., & Demoulin, P. 2004, ApJ, 617, 600
Gizon, L., Duvall, T. L., Jr., & Larsen, R. M. 2000, J. Astrophys. Astron., 21, 339
———. 2001, in IAU Symp. 203, Probing Surface Flows and Magnetic Activity with Time-Distance Helioseismology, ed. P. Brekke, B. Fleck, & J. B. Gurman (San Francisco: ASP), 189
Haber, D. A., Hindman, B. W., Toomre, J., Bogart, R. S., & Larsen, R. M. 2002, ApJ, 570, 855
Haber, D. A., Hindman, B. W., Toomre, J., Bogart, R. S., Schou, J., & Hill, F. 1998, in *SOHO* 6/GONG 98 Workshop, Structure and Dynamics of the Interior of the Sun and Sun-like Stars, ed. S. G. Korzennik & A. Wilson (ESA SP-418; Noordwijk: ESA), 791
Haber, D. A., Hindman, B. W., Toomre, J., Bogart, R. S., Thompson, M. J., & Hill, F. 2000, Sol. Phys., 192, 335
———. 2001, in Proc. *SOHO* 10/GONG 2000 Workshop, Helio- and Asteroseismology at the Dawn on the Millenium, ed. A. Wilson (ESA SP-464; Noodwijk: ESA), 209
Hagenaar, H. J., Schrijver, C. J., Title, A. M., & Shine, R. A. 1999, ApJ, 511, 932
Hathaway, D. H., Beck, J. G., Bogart, R. S., Bachmann, K. T., Khatri, G., Petitto, J. M., Han, S., & Raymond, J. 2000, Sol. Phys., 193, 299
Hindman, B. W., Gough, D., Thompson, M. J., & Toomre, J. 2005, ApJ, 621, 512
Karpen, J. T., Antiochos, S. K., Hohensee, M., & Klimchuk, J. A. 2001, ApJ, 553, L85
Karpen, J. T., Antiochos, S. K., Klimchuk, J. A., & MacNiece, P. J. 2003, ApJ, 593, 1187
Kippenhahn, R., & Schlüter, A. 1957, Z. Astrophys., 43, 36
Klimchuk, J. A. 2001, in Space Weather, ed. P. Song, H. J. Singer, & G. Siscoe (Geophys. Monogr. 125; Washington: AGU), 143
Kuijpers, J. 1997, ApJ, 489, L201
Kuperus, M., & Raadu, M. A. 1974, A&A, 31, 189
Lin, Y., Engvold, O., van der Voort, L. R., Wiik, J. E., & Berger, T. E. 2005, Sol. Phys., 226, 239
Low, B. C. 1993, ApJ, 409, 798
———. 2001, J. Geophys. Res., 106, 25141
Low, B. C., & Hundhausen, J. R. 1995, ApJ, 443, 818
MacKay, D. H., & van Ballegooijen, A. A. 2005, ApJ, 621, L77
Martens, P. C., & Zwaan, C. 2001, ApJ, 558, 872
Martin, S. F. 1998, Sol. Phys., 182, 107
———. 2000, Encyclopedia of Astronomy and Astrophysics, ed. P. Murdin (Bristol: IOP)
Martin, S. F., Bilimoria, R., & Tracadas, P. W. 1994, in Solar Surface Magnetism, ed. R. J. Rutten & C. J. Schrijver (NATO ASI Ser. C; Dordrect: Kluwer), 303
Moore, R. L. 2000, Encyclopedia of Astronomy and Astrophysics, ed. P. Murdin (Bristol: IOP)
Priest, E. R., Hood, A. W., & Anzer, U. 1989, ApJ, 344, 1010
Priest, E. R., van Ballegooijen, A. A., & MacKay, D. H. 1996, ApJ, 460, 530
Rust, D. M. 2000, Encyclopedia of Astronomy and Astrophysics, ed. P. Murdin (Bristol: IOP)
Rust, D. M., & Kumar, A. 1994, Sol. Phys., 155, 69
Scherrer, P. H., et al. 1995, Sol. Phys., 162, 129
Schrijver, C. J., et al. 1996, ApJ, 468, 921
Snodgrass, H. B. 1984, Sol. Phys., 94, 13
van Ballegooijen, A. A. 2001, Encyclopedia of Astronomy and Astrophysics, ed. P. Murdin (Bristol: IOP)
van Ballegooijen, A. A., Cartledge, N. P., & Priest, E. R. 1998, ApJ, 501, 866
van Ballegooijen, A. A., & Martens, P. C. H. 1989, ApJ, 343, 971
———. 1990, ApJ, 361, 283
van Ballegooijen, A. A., Priest, E. R., & MacKay, D. H. 2000, ApJ, 539, 983
Zhao, J., Kosovichev, A. G., Duvall, T. L., Jr. 2001, ApJ, 557, 384
Zirker, J. B. 2000, Encyclopedia of Astronomy and Astrophysics, ed. P. Murdin (Bristol: IOP)